

An actively stabilized, miniaturized epi-fluorescence widefield microscope for real-time observation in vivo

Ayiben Nuerbahati | Jiasheng Liao | Jing Lyu | Serk Abduwali | Li-Yang Chiang 

Dendrite Precision Medical Ltd, Tel Aviv-Jaffa, Israel

CorrespondenceLi-Yang Chiang, Dendrite Precision Medical Ltd., Berkowitz St., Tel Aviv-Jaffa, Israel.
Email: johnny@scellmed.com**Funding information**

Dendrite Precision Medical Ltd.

Review Editor: Alberto Diaspro**Abstract**

Recent developments in real-time, in vivo micro-imaging have allowed for the visualization of tissue pathological changes, facilitating rapid diagnosis. However, miniaturization, magnification, the field of view, and in vivo image stabilization remain challenging factors to reconcile. A key issue for this technology is ensuring it is user friendly for surgeons, enabling them to use the device manually and obtain instantaneous information necessary for surgical decision-making. This descriptive study introduces a handheld, actively stabilized, miniaturized epi-fluorescence widefield microscope (MEW-M) for real-time observation in vivo with high resolution. The methodology of MEW-M system includes high resolution microscopy miniaturization technology, thousandfold shaking suppression (actively stabilized), ultra-photosensitivity, and tailored image signal processing cell image capture and processing technology, which support for the excellent real-time imaging performance of MEW-M system in brain, mammary, liver, lung, and kidney tissue imaging of rats in vivo. With a single-objective and high-frame-rate imaging, the MEW-M system facilitates roving image acquisition, enabling contiguous analysis of large tissue areas.

Research Highlights A handheld, actively stabilized MEW-M system was introduced. Excellent real-time, in vivo imaging with high resolution and active stabilization in brain, mammary, liver, lung, and kidney tissue of rats.

KEYWORDS

actively stabilized, epi-fluorescence microscope, handheld, imaging, in vivo, real-time observation, widefield

1 | INTRODUCTION

The development of accurate, robust, and user-friendly point-of-care diagnostic or real-time imaging devices that are small, portable, and affordable is crucial. Optical imaging techniques play a critical role in achieving such technologies by providing high-resolution diagnostic or observational information in a minimally invasive or noninvasive manner. Oh et al. (2018) reported the real-time optical imaging used in the diagnosis of microbubble destruction in microfluidic capillary. Sung et al. (2021) performed a phase II multicenter trial for optical coherence tomography using an intravesical real time imaging and staging of bladder cancer. In addition, the use of miniature and flexible optical

components enables cellular-level imaging to be performed alongside standard widefield methods such as endoscopy, enabling access to tissue in confined areas of the body. Studies have investigated the application of these types of microscopes for their potential use in real-time imaging (Jean et al., 2007; Lane et al., 2009; Muldoon et al., 2007), screening (Muldoon et al., 2008), clinical diagnostics (Carlson et al., 2005; Zhong et al., 2009), and surgical guidance (Muldoon et al., 2008; Zhong et al., 2009).

High- or super-resolution optical imaging techniques for investigating deep tissues are currently limited to in vitro cell cultures or tissue slices due to the attenuation of light propagation caused by scattering and absorption (Jung et al., 2004; Wilt et al., 2009).

Two-photon fluorescence microscopy takes advantage of the penetration ability of near-infrared light and objectives with high numerical aperture (NA) to enable three-dimensional tissue imaging as deep as 500–1000 μm with cellular-level resolution (Gu et al., 2014; Helmchen & Denk, 2005; Theer et al., 2003). Several strategies, such as improving fluorescence signal generation, optical signal collection, and endoscope use, have been proposed to extend the penetration depth of this technique (Wilt et al., 2009). In a previous study, a miniaturized endoscopic objective with a tip diameter of only 3 mm was used for minimally invasive *in vivo* observation of deep tissue (Feng et al., 2019). Endoscope-based approaches, which are compatible with matured optical microscope technologies such as widefield epifluorescence, laser-scanning confocal, and two-photon fluorescence, provide an effective way to achieve *in vivo* observation deeper than 1000 μm (Barretto et al., 2009; Barretto et al., 2011; Flusberg et al., 2008; Kim et al., 2010). By combining these microscopy methods with gradient refractive index lenses commonly used in endoscopy, researchers have achieved *in vivo* fluorescence imaging in various tissues, including muscle (Llewellyn et al., 2008; Prajapati et al., 2010), digestive tract (Lee & Wang, 2016), vasculature (Yang et al., 2011), hippocampus (Turtaev et al., 2018), and nervous system (Samarasena et al., 2016; Yashiro et al., 2017). However, the use of polymer-based materials can result in autofluorescence, which reduces image quality compared with glass-based objectives.

However, while current fluorescence imaging microscope technology has been used in clinical practice, such as activated neutrophil optical fluorescent imaging in human lungs (Craven et al., 2021), intraoperative fluorescence imaging of colorectal cancer (de Valk et al., 2021), there remain some issues that need to be addressed, including operator-induced shaking and physiological fibrillation (Acerbi et al., 2020; Belderbos et al., 2017; Martirosyan et al., 2016) (such as blood vessel pulsation, breathing and muscle pulsation) in patients, both of which can result in degraded image quality. Although using a mechanical fixed arm instead of hand-holding can alleviate some of the shaking, it is not as convenient as handheld use. By using a widefield epi-fluorescence arrangement instead of point-scanning, the system complexity and cost are greatly reduced. When used with bright, fluorescent contrast agents, subcellular morphology can be viewed in real time, by simply placing the distal end of the objective onto the tissue site to be imaged. Therefore, this study aimed to describe an actively stabilized, miniaturized epi-fluorescence widefield microscope (MEW-M) system, which might be potential in real-time observation in tissue resection.

2 | METHODS AND MATERIALS

2.1 | Overview of the MEW-M system

The MEW-M system is an endomicroscopic scanner for cellular structure, abbreviated as EndoSCell. Based on a handheld modification (Zhang et al., 2021) and the MEW-W, the MEW-M system successfully achieves active stabilization, maintains real-time extreme optical

image stabilization (OIS), removes the robotic arm and allows direct hand-holding, and provides a 550–1500 \times magnification for *in vivo* imaging (Figure 1a,b), which allow this system being capable of portable histopathological microscopy with optical performance comparable to a conventional histopathological microscope in terms of field of view (FOV) and lateral resolution. MEW-M system is immune to vibration caused by hand shaking due to its anti-shake design, which revolves around a module for shifting the image sensor (Figure 1c). These indicate that MEW-M system can be used to carry out intraoperative histological observation *in situ* and *in vivo*, and investigate living tissues at submicron/subcellular level in real time. It has a diameter of 4 mm, a length of 22 cm, and can reach a lateral resolution of 0.67 μm , allowing for observation of subcellular organelles such as dendrites, nuclei, nucleolus, and nuclear-cytoplasmic ratio, which are typically used for histopathological diagnosis (Figure 1d, e).

2.2 | Testing of optics

MEW-M system boasts a 100 μm penetration depth and operates at a frame rate of 60 Hz. This configuration facilitates the observation of four to five cell layers within a relatively expansive FOV measuring 500 μm and supports for providing very stable real-time images from living tissues. Functioning as a contact microscope, MEW-M system eliminates the need for manual focusing adjustments. Remarkably, it captures dynamic images from moving objects in a mere 16 ms. The small objective, featuring a NA of 0.5, comprises a composition of nine lenses. Among the nine lenses, one surface is distinctly super-hemispherical, whereas several surfaces approximate a hemispherical shape. The smallest objective lens size is Φ 0.8 mm, and the most compact radius of curvature is at R 0.8 mm (Figure 2a).

As a minimal aberration system, MEW-M system mandates rigorous manufacturing tolerances to uphold lens precision. Peak-to-valley (PV) of the spherical and astigmatism irregularity is required to achieve a resolution of 1/20 wavelength. The eccentric tolerance of components is required to be less than 5 μm . The position tolerance between glass lenses and center thickness tolerance is required to be less than 5 μm . The entire assembly is required to be completed in a stress-free state. To ensure the signal-to-noise ratio of fluorescence imaging, all glass materials are required to be non-autofluorescent. The lens is a microscopic endoscope with a stainless-steel tube outer diameter of only 4 mm, with NA 0.50 and 12 \times magnification (Figure 2b). The object FOV is 0.5 mm. The object image conjugate distance is 221 mm. The imaging spectrum spans from 480 to 600 nm. Notably, the modulation transfer function cutoff frequency of the lens is greater than 1500 lp/mm, and the central field wave aberration PV value is less than 1/10 λ (Figure 2c). The axial chromatic aberration at an aperture of 0.707 is less than one focus depth. The chromatic spherical aberration is less than twice the depth. The vertical chromatic aberration in different fields of view is all within the Airy disk. Field curvature and astigmatism at the edge of the FOV are less than one focal depth. The optical parameters

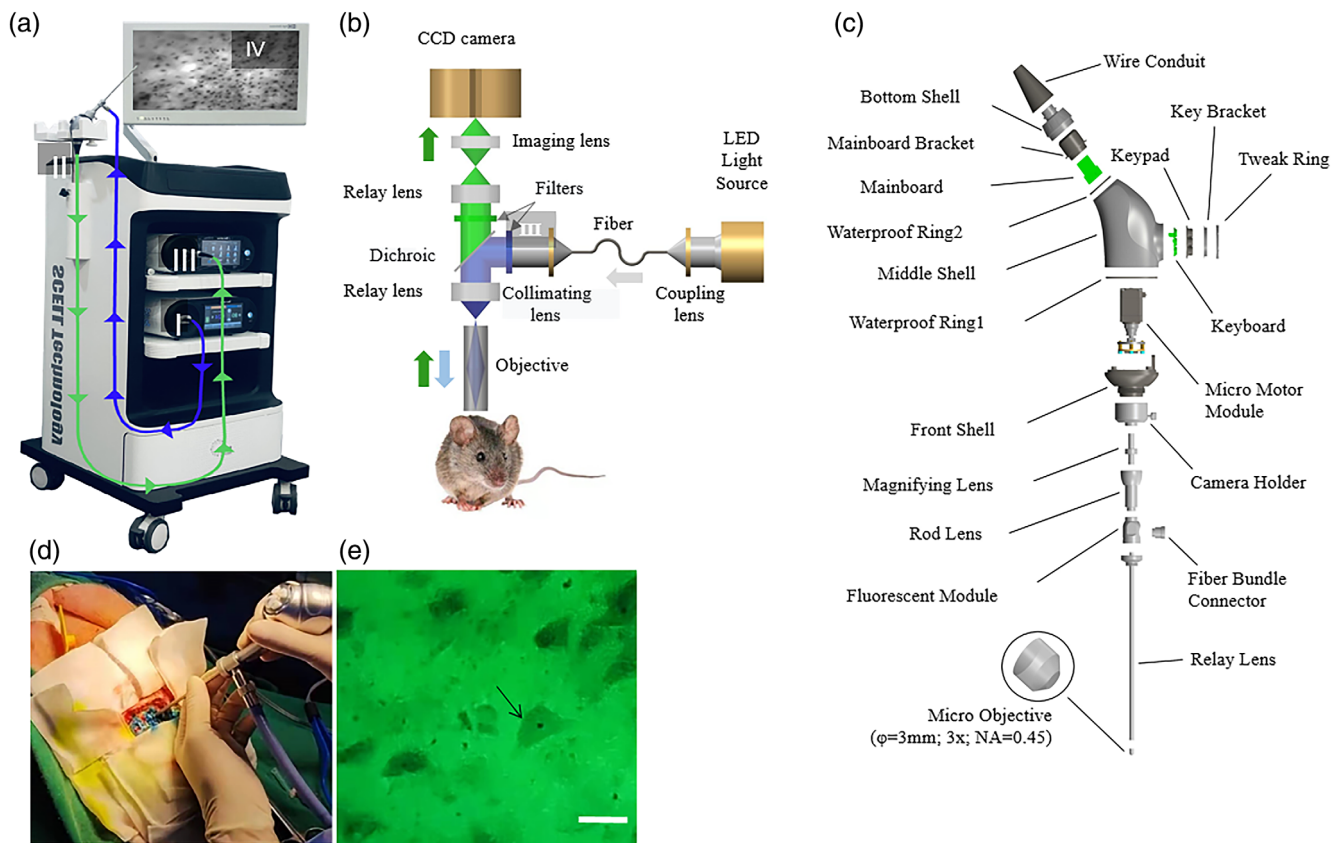


FIGURE 1 Design and assembly of miniaturized epi-fluorescence widefield microscope (MEW-M) system. (a) System schematic shows the major modules of MEW-M: LED light source (I), camera readout (II), data acquisition system (III), and monitor (IV). (b) The optical path of MEW-M resembles a conventional epi-fluorescence microscope. (c) MEW-M optics consist of numerous components, among which a high-end micro-objective ($\Phi = 3 \text{ mm}$; $3\times$; $NA = 0.45$) and an anti-shake module are the key components. (d) A neurosurgeon holding the lens of MEW-M system to investigate a pig brain in vivo. (e) In vivo micrograph shows pyramidal cells from pig cortical region with clear dendrites and nucleolus (yellow arrow, scale bar is $50 \mu\text{m}$). CCD, charge coupled device; LED, light-emitting diode.

of the MEW-E system are shown in Figures S1–S11. The optical performance of MEW-M system is provided in Figure 2d,e.

2.3 | Architecture of microscopic image stabilization technology

The image sensor shifting capabilities include four trapezoidal magnets, four OIS coils, two position sensors (Sharma et al., 2019), and a voice coil motor (VCM) (Hsieh et al., 2020) actuator configured to shift an image sensor along multiple axes. The image sensor is equipped with a magnet and coil configuration, incorporating multiple magnets. Each magnet is paired with its own OIS coil and additional autofocus (AF) coil (s) positioned either above or below the magnets. Furthermore, a flexure arrangement suspended a coil carrier assembly holding the OIS and AF coils and a substrate holding the image sensor. Current can be driven in a controlled manner through the coils to move the coil carrier assembly and substrate to shift the image sensor for OIS and/or AF.

As shown in Figure 3a, the main components of our proposed anti-shake technology are a complementary metal-oxide-semiconductor (CMOS)

transistor, magnet, position sensor, VCM, metal wire, printed circuit board, and reed. The workflow is shown in Figure 3b. In addition, an endoscope is used to obtain real-time images, and position sensors (specifically, linear Hall sensors) are used to detect the direction and amplitude of vibration of the endoscope in real time. A field programmable gate array (FPGA) clock is used to simultaneously collect the data acquired by the position sensor, image sensor, and VCM, and the data are processed at a clock rate of 40 MHz, that is, 25 ns, to obtain the direction, speed, and displacement of the vibration. Then, the movement of the CMOS sensor required to offset the vibration is calculated. The logic control sequence is designed according to the calculated movement compensation. Furthermore, multiple sequence flows are used to accurately control the flow direction of the current in the coil at the nanosecond level to attract or repel the corresponding magnet, thereby producing relative motion between the coil and the magnet. The movement compensation of the image sensor in the x-y plane and the AF motion in the z direction orthogonal to the optical axis are realized by the current-driven coil, thereby achieving image stabilization and AF.

Figure 3c illustrates the displacement-based OIS structure. Compensation motion for stabilization is performed by a magnet-controlled system (Figure 3d). When an image is out of focus, FPGA calculates the sharpness evaluation function at a high speed

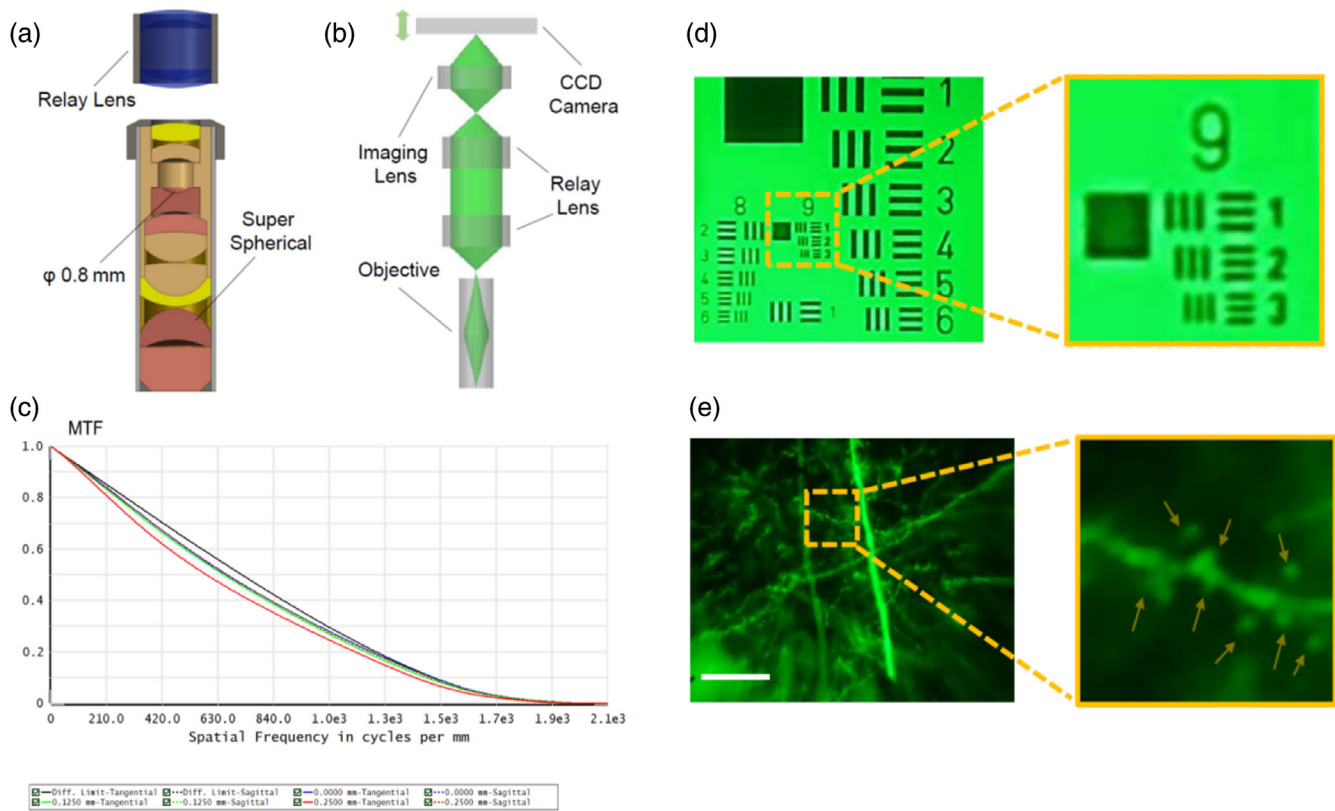


FIGURE 2 Optical performance of miniaturized epi-fluorescence widefield microscope (MEW-M) system, confirming submicron, subcellular resolution. (a) Internal structure of the micro-objective from MEW-M. (b) The optical path. (c) Modulation transfer function (MTF) of MEW-M optics. (d) The third element of the last group (Group 9) of the 1951 USAF target, imaged by MEW-M system. The width of the smallest resolved bar in the inset is $0.77 \mu\text{m}$, corresponding to $F_{\text{max}} = 645 \text{ lp/mm}$. (e) MEW-M system micrograph from brain slice of Thy1-YFP mouse shows the robust formation of the subcellular functional regions, namely, the dendritic spines, which are normally $0.5 \mu\text{m}$ ($0.1\text{--}1 \mu\text{m}$) in diameter (scale bar = $100 \mu\text{m}$). CCD, charge coupled device.

and maps it to the current of the VCM coil. Because of the presence of the magnetic field of the AF coil, the CMOS sensor substrate moves in a straight line (Figure 3e), and the upper and lower leaf spring are used to maintain the stability of the substrate. With anti-shake technology in place, surgeons can hold the lens of MEW-M system in hand (Figure 3f) and observe neuronal cells from the surgical margin without interference from vibration (Figure 3g,h).

3 | RESULTS

3.1 | Evidence for active stabilization

A vibration of 2.5 mm (By comparing the range of pixels covered by the size of the marker, the distance represented by each pixel was determined. The range of shaking is determined by comparing the pixels moved by the mark point in each frame. The maximum shaking in the video was computed to be 2.5 mm) caused by involuntary shaking of the hand was recorded, and this vibration was eliminated by the anti-shake technology, resulting in an average of $4 \mu\text{m}$ cellular offset (Video S1, imaging of rat liver/kidney/brain tissue). A $4 \mu\text{m}$ cellular offset is negligible, confirming the

usefulness of the actively stabilized technology. The handheld shaking range is on the millimeter scale, while the shaking seen at the cellular level through the lens of MEW-M system is on the micron scale. Since the MEW-M system has a 1000-fold magnification, it can assume that the shaking caused by hand-holding should theoretically reach 1 meter after being amplified by 1000-fold. However, the actively stabilized design (thousandfold shaking suppression) of MEW-M system can reduce this theoretical value to the micron level.

3.2 | In vivo brain, mammary, liver, lung, and kidney tissue imaging from rat

To assess the application of MEW-M system in vivo imaging preliminarily, this study conducted experiment of in vivo imaging observations by MEW-M system in multiple organs of rats, including the brain, mammary gland, liver, lung, and kidney. After anesthetizing the rats, local incisions were made to expose the target organs, and then, the MEW-M system was employed in tissue imaging after staining with 0.25% fluorescein sodium (Sigma-Aldrich, Inc, USA) for 2 min and 4% methylene blue (Sigma-Aldrich, Inc, USA) for another 2 min,

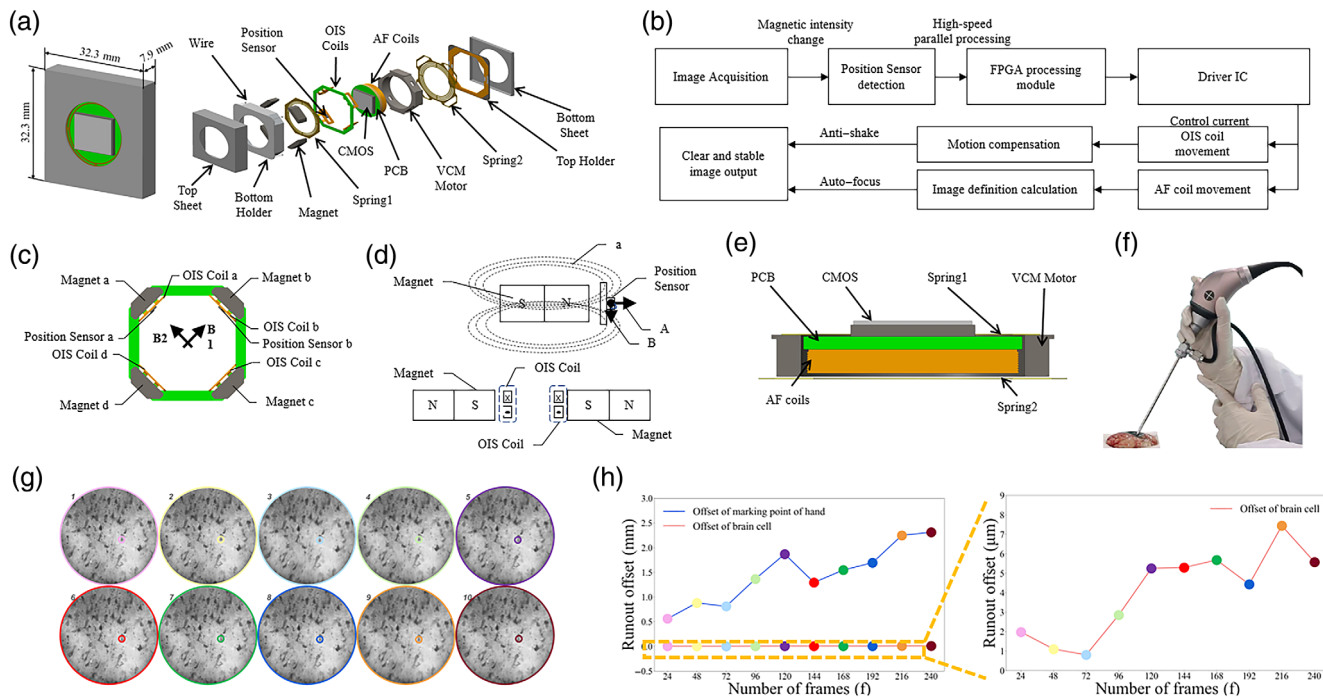


FIGURE 3 Architecture and performance test of the anti-shake technology. (a) 3D diagram of system structure. (b) Actively stabilized architecture flowchart. (c) The image sensor shifting structure. (d) Schematic of the correspondence between the position sensor and the magnet. (e) Autofocus (AF) structure diagram. (f) Example picture showing intraoperative use of the miniaturized epi-fluorescence widefield microscope system by hand to scan through brain samples from pig. (g) Over 4 s, a vibration of approximately 2.5 mm was caused by involuntary shaking of the hand. (h) Micrographs from pig brain samples over 4 s observation show clear and stable images. (i) Over 4 s, a maximum 8 μm shift (as compared with 2.5 mm vibration without anti-shake technology) was recorded from cellular level micrographs, confirming a very stable image due to anti-shake technology. CMOS, complementary metal-oxide-semiconductor; FPGA, field-programmable gate array; OIS, optical image stabilization; PCB, printed circuit board; VCM, voice coil motor.

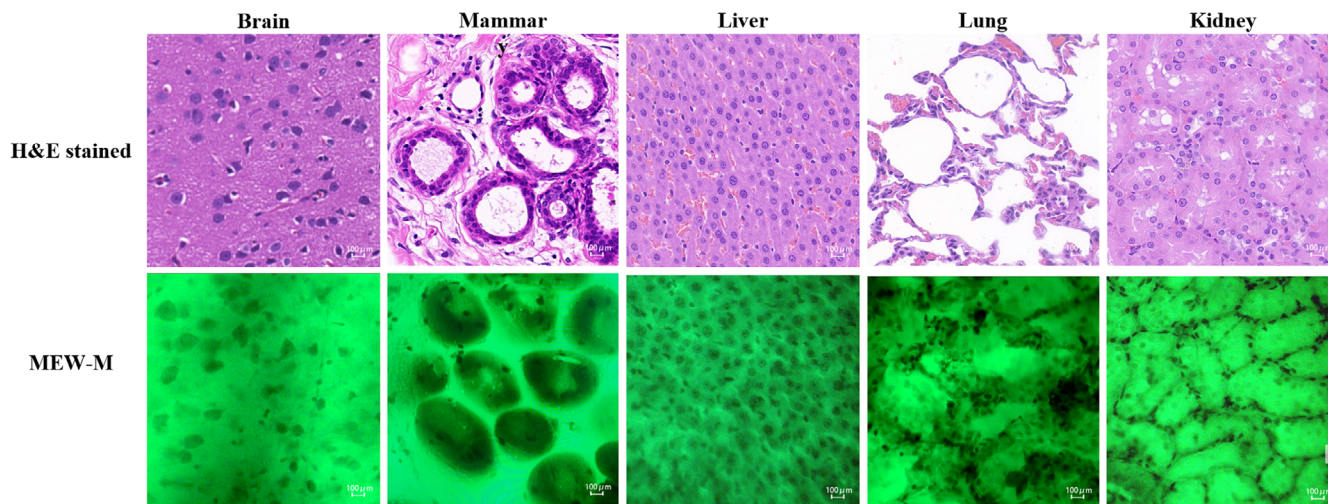


FIGURE 4 Imaging of organs tissue in rat, including brain, mammary, liver, lung, and kidney. The upper panel was H&E stained histological examination, and the lower panel was image of endoscopic examination of miniaturized epi-fluorescence widefield microscope (MEW-M) system in vivo.

each followed by a rinse with physiological saline. As shown in Figure 4, the MEW-M system in vivo images can clearly display the tissue and cellular structures of multiple organs with excellent clarity and contrast.

4 | DISCUSSION

This study indicated that the actively stabilized MEW-M system has favorable real-time imaging performance in brain, mammary, liver,

lung, and kidney tissue imaging of rat *in vivo*, which might be applied in real-time observation in tissue resection.

MEW-M system is a handheld microscope designed for *in vivo* use that provides a miniaturized solution with a diameter of less than 4 mm and a weight of less than 100 g. With a 550–1500 \times magnification, 500 μ m FOV, 100 μ m penetration depth, and 0.5 μ m resolution, it offers superior optical performance compared with existing technologies like Endocyt or narrow-band imaging (NBI) from OLYMPUS (450–1100 \times magnification), and the confocal endomicroscopy (CLE)-based system (380–600 \times magnification) (Jin et al., 2008; Kitabatake et al., 2006; Neumann et al., 2011), which are highly invasive for neurosurgeries and have a much larger distal end outer diameter (9.7–12.8 mm). The Endocyt or NBI from OLYMPUS are mainly used for real-time observation of the interior of organ cavities through natural orifices, such as for colorectal cancer detection (Sano et al., 2016). The CLE-based systems require much longer imaging time, often involving 70 images per specimen and 15 min per patient, as well as additional affixation tools, such as gentle suction and a probe holder (De Palma et al., 2010; Martirosyan et al., 2016). In contrast, the MEW-M system's acquisition frame rate allows for much shorter imaging time, meaning total coverage of a large centimeter square area of examination would only take a few seconds.

While not yet available on a routine basis, utilizing a technique like the MEW-M system for neurosurgical procedures could improve tumor visualization at the margin and speed up intraoperative diagnosis. Some studies have found CLE-based imaging systems to have comparable specificity and sensitivity to frozen sections for providing diagnostic information during biopsy or resection of human brain tumors (Belykh et al., 2016; Belykh et al., 2019; Eschbacher et al., 2012; Osman et al., 2018). However, current CLE-based and Raman-based imaging microscope systems developed for neurosurgical use still have limitations, such as unoptimized image processing and display, low ergonomic position of the handheld probe, and a lack of sterile attachments for the imaging probe (Eschbacher et al., 2012; Hollon et al., 2016; Martirosyan et al., 2014). Additionally, traditional *in vivo* imaging microscopes, such as the two-photon microscope, require a vibration-isolation table and a mechanical arm to prevent shaking. Raman-based microscopic images also have a limited signal-to-noise ratio and are complicated to interpret (Tao et al., 2012). However, the MEW-M system has an actively stabilized mechanism which reduces mechanical interference from hand shaking, that is not currently available with other real-time *in vivo* imaging microscopes.

In conclusion, this study suggests that the MEW-M system has the potential to be a surgeon-friendly, rapid, and cost-effective alternative to conventional histopathology and microendoscopy, providing real-time intraoperative feedback to facilitate closed loop treatment decisions in clinical practice. This includes accurate assessment of surgical margins and comprehensive surveillance of large tissue areas to guide biopsy site selection without the need for permanent tissue damage or removal. Nevertheless, the clinical application of the MEW-M system still requires further confirmation through large-scale prospective studies with a large clinical sample size.

AUTHOR CONTRIBUTIONS

Ayiben Nuerbahati: Data curation; writing. **Jiasheng Liao:** Formal analysis; data curation. **Jing Lyu:** Data curation; formal analysis. **Serk Abduwali:** Formal analysis; data curation. **Li-Yang Chiang:** Data curation; formal analysis; writing – review and editing; writing – original draft; conceptualization.

ACKNOWLEDGMENTS

Thanks to Suzhou Institute of Biomedical Engineering and Technology Chinese Academy of Sciences for providing Zemax software for optical simulation and design verification.

FUNDING INFORMATION

This study was funded by Dendrite Precision Medical Ltd., Berkowitz St., Tel Aviv-Jaffa, Israel.

CONFLICT OF INTEREST STATEMENT

The authors declare no conflicts of interest.

DATA AVAILABILITY STATEMENT

The data that support the findings of this study are available on request from the corresponding author. The data are not publicly available due to privacy or ethical restrictions.

ORCID

Li-Yang Chiang  <https://orcid.org/0009-0000-7872-682X>

REFERENCES

- Acerbi, F., Pollo, B., De Laurentis, C., Restelli, F., Falco, J., Vetrano, I. G., Broggi, M., Schiariti, M., Tramacere, I., Ferroli, P., & DiMeco, F. (2020). *Ex vivo* fluorescein-assisted confocal laser endomicroscopy (CONVIVO[®] system) in patients with glioblastoma: Results from a prospective study. *Frontiers in Oncology*, 23(10), 606574. <https://doi.org/10.3389/fonc.2020.606574>
- Barretto, R. P., Ko, T. H., Jung, J. C., Wang, T. J., Capps, G., Waters, A. C., Ziv, Y., Attardo, A., Recht, L., & Schnitzer, M. J. (2011). Time-lapse imaging of disease progression in deep brain areas using fluorescence microendoscopy. *Nature Medicine*, 17(2), 223–228. <https://doi.org/10.1038/nm.2292>
- Barretto, R. P., Messerschmidt, B., & Schnitzer, M. J. (2009). *In vivo* fluorescence imaging with high-resolution microlenses. *Nature Methods*, 6(7), 511–512. <https://doi.org/10.1038/nmeth.1339>
- Belderbos, T. D. G., van Oijen, M. G. H., Moons, L. M. G., & Siersema, P. D. (2017). Implementation of real-time probe-based confocal laser endomicroscopy (pCLE) for differentiation of colorectal polyps during routine colonoscopy. *Endoscopy International Open*, 5(11), E1104–E1110. <https://doi.org/10.1055/s-0043-117948>
- Belykh, E., Martirosyan, N. L., Yagmurlu, K., Miller, E. J., Eschbacher, J. M., Izadyazdanabadi, M., Bardanova, L. A., Byvaltsev, V. A., Nakaji, P., & Preul, M. C. (2016). Intraoperative fluorescence imaging for personalized brain tumor resection: Current state and future directions. *Frontiers in Surgery*, 17(3), 55. <https://doi.org/10.3389/fsurg.2016.00055>
- Belykh, E., Miller, E. J., Carotenuto, A., Patel, A. A., Cavallo, C., Martirosyan, N. L., Healey, D. R., Byvaltsev, V. A., Scheck, A. C., Lawton, M. T., Eschbacher, J. M., Nakaji, P., & Preul, M. C. (2019). Progress in confocal laser endomicroscopy for neurosurgery and technical nuances for brain tumor imaging with fluorescein. *Frontiers in Oncology*, 3(9), 554. <https://doi.org/10.3389/fonc.2019.00554>

- Carlson, K., Pavlova, I., Collier, T., Descour, M., Follen, M., & Richards-Kortum, R. (2005). Confocal microscopy: Imaging cervical precancerous lesions. *Gynecologic Oncology*, 99(3 Suppl 1), S84–S88. <https://doi.org/10.1016/j.ygyno.2005.07.049>
- Craven, T. H., Walton, T., Akram, A. R., Scholefield, E., McDonald, N., Marshall, A. D. L., Humphries, D. C., Mills, B., Campbell, T. A., Bruce, A., Mair, J., Dear, J. W., Newby, D. E., Hill, A. T., Walsh, T. S., Haslett, C., & Dhaliwal, K. (2021). Activated neutrophil fluorescent imaging technique for human lungs. *Scientific Reports*, 11(1), 976. <https://doi.org/10.1038/s41598-020-80083-w>
- De Palma, G. D., Staibano, S., Siciliano, S., Persico, M., Masone, S., Maione, F., Siano, M., Mascolo, M., Esposito, D., Salvatori, F., & Persico, G. (2010). In vivo characterisation of superficial colorectal neoplastic lesions with high-resolution probe-based confocal laser endomicroscopy in combination with video-mosaicing: A feasibility study to enhance routine endoscopy. *Digestive and Liver Disease*, 42(11), 791–797. <https://doi.org/10.1016/j.dld.2010.03.009>
- de Valk, K. S., Deken, M. M., Schaap, D. P., Meijer, R. P., Boogerd, L. S., Hoogstins, C. E., van der Valk, M. J., Kamerling, I. M., Bhairosingh, S. S., Framery, B., Hilling, D. E., Peeters, K. C., Holman, F. A., Kusters, M., Rutten, H. J., Cailler, F., Burggraaf, J., & Vahrmeijer, A. L. (2021). Dose-finding study of a CEA-targeting agent, SGM-101, for intraoperative fluorescence imaging of colorectal cancer. *Annals of Surgical Oncology*, 28(3), 1832–1844. <https://doi.org/10.1245/s10434-020-09069-2>
- Eschbacher, J., Martirosyan, N. L., Nakaji, P., Sanai, N., Preul, M. C., Smith, K. A., Coons, S. W., & Spetzler, R. F. (2012). In vivo intraoperative confocal microscopy for real-time histopathological imaging of brain tumors. *Journal of Neurosurgery*, 116(4), 854–860. <https://doi.org/10.3171/2011.12.JNS11696>
- Feng, Z., Yu, X., Jiang, M., Zhu, L., Zhang, Y., Yang, W., Xi, W., Li, G., & Qian, J. (2019). Excretable IR-820 for in vivo NIR-II fluorescence cerebrovascular imaging and photothermal therapy of subcutaneous tumor. *Theranostics*, 9(19), 5706–5719. <https://doi.org/10.7150/thno.31332>. Erratum in: *Theranostics*. 2022 Nov 2;12(17):7640.
- Flusberg, B. A., Nimmerjahn, A., Cocker, E. D., Mukamel, E. A., Barretto, R. P., Ko, T. H., Burns, L. D., Jung, J. C., & Schnitzer, M. J. (2008). High-speed, miniaturized fluorescence microscopy in freely moving mice. *Nature Methods*, 5(11), 935–938. <https://doi.org/10.1038/nmeth.1256>
- Gu, M., Kang, H., & Li, X. (2014). Breaking the diffraction-limited resolution barrier in fiber-optical two-photon fluorescence endoscopy by an azimuthally-polarized beam. *Scientific Reports*, 10(4), 3627. <https://doi.org/10.1038/srep03627>
- Helmchen, F., & Denk, W. (2005). Deep tissue two-photon microscopy. *Nature Methods*, 2(12), 932–940. <https://doi.org/10.1038/nmeth818>. Erratum in: *Nature Methods*. 2006 Mar;3(3):235.
- Hollon, T., Lewis, S., Freudiger, C. W., Sunney Xie, X., & Orringer, D. A. (2016). Improving the accuracy of brain tumor surgery via Raman-based technology. *Neurosurgical Focus*, 40(3), E9. <https://doi.org/10.3171/2015.12.FOCUS15557>
- Hsieh, C.-L., Liu, C.-S., & Cheng, C.-C. (2020). Design of a 5 degree of freedom-voice coil motor actuator for smartphone camera modules. *Sensors and Actuators A: Physical*, 309, 112014. <https://doi.org/10.1016/j.sna.2020.112014>
- Jean, F., Bourg-Heckly, G., & Viellerobe, B. (2007). Fibered confocal spectroscopy and multicolor imaging system for in vivo fluorescence analysis. *Optics Express*, 15(7), 4008–4017. <https://doi.org/10.1364/oe.15.004008>
- Jin, H., Gang, S., & Yun-Sheng, Y. (2008). Research status of confocal microendoscopy. *Journal of World Chinese Digestion*, 16(25), 2867–2870.
- Jung, J. C., Mehta, A. D., Aksay, E., Stepnoski, R., & Schnitzer, M. J. (2004). In vivo mammalian brain imaging using one- and two-photon fluorescence microendoscopy. *Journal of Neurophysiology*, 92(5), 3121–3133. <https://doi.org/10.1152/jn.00234.2004>
- Kim, P., Chung, E., Yamashita, H., Hung, K. E., Mizoguchi, A., Kucherlapati, R., Fukumura, D., Jain, R. K., & Yun, S. H. (2010). In vivo wide-area cellular imaging by side-view endomicroscopy. *Nature Methods*, 7(4), 303–305. <https://doi.org/10.1038/nmeth.1440>
- Kitabatake, S., Niwa, Y., Miyahara, R., Ohashi, A., Matsuura, T., Iguchi, Y., Shimoyama, Y., Nagasaka, T., Maeda, O., Ando, T., Ohmiya, N., Itoh, A., Hirooka, Y., & Goto, H. (2006). Confocal endomicroscopy for the diagnosis of gastric cancer in vivo. *Endoscopy*, 38(11), 1110–1114. <https://doi.org/10.1055/s-2006-944855>
- Lane, P. M., Lam, S., McWilliams, A., Leriche, J. C., Anderson, M. W., & Macaulay, C. E. (2009). Confocal fluorescence microendoscopy of bronchial epithelium. *Journal of Biomedical Optics*, 14(2), 024008. <https://doi.org/10.1117/1.3103583>
- Lee, J. H., & Wang, T. D. (2016). Molecular endoscopy for targeted imaging in the digestive tract. *The Lancet Gastroenterology & Hepatology*, 1(2), 147–155. [https://doi.org/10.1016/S2468-1253\(16\)30027-9](https://doi.org/10.1016/S2468-1253(16)30027-9)
- Llewellyn, M. E., Barretto, R. P., Delp, S. L., & Schnitzer, M. J. (2008). Minimally invasive high-speed imaging of sarcomere contractile dynamics in mice and humans. *Nature*, 454(7205), 784–788. <https://doi.org/10.1038/nature07104>
- Martirosyan, N. L., Eschbacher, J. M., Kalani, M. Y., Turner, J. D., Belykh, E., Spetzler, R. F., Nakaji, P., & Preul, M. C. (2016). Prospective evaluation of the utility of intraoperative confocal laser endomicroscopy in patients with brain neoplasms using fluorescein sodium: Experience with 74 cases. *Neurosurgical Focus*, 40(3), E11. <https://doi.org/10.3171/2016.1.FOCUS15559>
- Martirosyan, N. L., Georges, J., Eschbacher, J. M., Cavalcanti, D. D., Elhadi, A. M., Abdelwahab, M. G., Scheck, A. C., Nakaji, P., Spetzler, R. F., & Preul, M. C. (2014). Potential application of a hand-held confocal endomicroscope imaging system using a variety of fluorophores in experimental gliomas and normal brain. *Neurosurgical Focus*, 36(2), E16. <https://doi.org/10.3171/2013.11.FOCUS13486>
- Muldoon, T. J., Anandasabapathy, S., Maru, D., & Richards-Kortum, R. (2008). High-resolution imaging in Barrett's esophagus: A novel, low-cost endoscopic microscope. *Gastrointestinal Endoscopy*, 68(4), 737–744. <https://doi.org/10.1016/j.gie.2008.05.018>
- Muldoon, T. J., Pierce, M. C., Nida, D. L., Williams, M. D., Gillenwater, A., & Richards-Kortum, R. (2007). Subcellular-resolution molecular imaging within living tissue by fiber microendoscopy. *Optics Express*, 15(25), 16413–16423. <https://doi.org/10.1364/oe.15.016413>
- Neumann, H., Fuchs, F. S., Vieth, M., Atreya, R., Siebler, J., Kiesslich, R., & Neurath, M. F. (2011). Review article: In vivo imaging by endocytoscopy. *Alimentary Pharmacology & Therapeutics*, 33(11), 1183–1193. <https://doi.org/10.1111/j.1365-2036.2011.04647.x>
- Oh, M. T., Kim, H. N., Ko, H. S., Lee, S., Kim, J. H., & Lee, B. C. (2018). Real-time optical imaging of microbubble destruction with an acoustic lens attached ultrasonic diagnostic probe in microfluidic capillary models. In: *Annual international conference of the IEEE engineering in medicine and biology society* (pp. 6068–6071). IEEE, Honolulu, HI, USA. <https://doi.org/10.1109/EMBC.2018.8513590>
- Osman, H., Georges, J., Elsayh, D., Hattab, E. M., Yocom, S., & Cohen-Gadol, A. A. (2018). In vivo microscopy in neurosurgical oncology. *World Neurosurgery*, 115, 110–127. <https://doi.org/10.1016/j.wneu.2018.03.218>
- Prajapati, S. I., Martinez, C. O., Abraham, J., McCleish, A. T., Michalek, J. E., McManus, L. M., Rubin, B. P., Shireman, P. K., & Keller, C. (2010). Crimson carrier, a long-acting contrast agent for in vivo near-infrared imaging of injured and diseased muscle. *Muscle & Nerve*, 42(2), 245–251. <https://doi.org/10.1002/mus.21682>
- Samarasena, J. B., Ahluwalia, A., Shinoura, S., Choi, K. D., Lee, J. G., Chang, K. J., & Tarnawski, A. S. (2016). In vivo imaging of porcine gastric enteric nervous system using confocal laser endomicroscopy & molecular neuronal probe. *Journal of Gastroenterology and Hepatology*, 31(4), 802–807. <https://doi.org/10.1111/jgh.13194>
- Sano, Y., Tanaka, S., Kudo, S. E., Saito, S., Matsuda, T., Wada, Y., Fujii, T., Ikematsu, H., Uraoka, T., Kobayashi, N., Nakamura, H., Hotta, K.,

- Horimatsu, T., Sakamoto, N., Fu, K. I., Tsuruta, O., Kawano, H., Kashida, H., Takeuchi, Y., ... Saito, Y. (2016). Narrow-band imaging (NBI) magnifying endoscopic classification of colorectal tumors proposed by the Japan NBI expert team. *Digestive Endoscopy*, 28(5), 526–533. <https://doi.org/10.1111/den.12644>
- Sharma, S., Francisco, S., Miller, S. W., & Gatos, L. (2019). *Camera with image sensor shifting* (U.S. Patent No. 20190020822). Al. 2019-1-17.
- Sung, H. H., Scherr, D. S., Slaton, J., Liu, H., Feeny, K. L., Lingley-Papadopoulos, C., Gearheart, J., Zara, J. M., & Lerner, S. P. (2021). Phase II multi-center trial of optical coherence tomography as an adjunct to white light cystoscopy for intravesical real time imaging and staging of bladder cancer. *Urologic Oncology*, 39(7), 434.e23–434.e29. <https://doi.org/10.1016/j.urolonc.2021.03.026>
- Tao, C., Zhilong, Y., Xiannian, Z., Xiaoliang, X., & Yanyi, H. (2012). Coherent Raman scattering microscopy. *Science in China: Chemistry*, 42(1), 1–16. www.scichina.com/chem.scichina.com
- Theer, P., Hasan, M. T., & Denk, W. (2003). Two-photon imaging to a depth of 1000 microm in living brains by use of a Ti: Al₂O₃ regenerative amplifier. *Optics Letters*, 28(12), 1022–1024. <https://doi.org/10.1364/ol.28.001022>
- Turtaev, S., Leite, I. T., Altwegg-Boussac, T., Pakan, J. M. P., Rochefort, N. L., & Čižmár, T. (2018). High-fidelity multimode fibre-based endoscopy for deep brain in vivo imaging. *Light, Science & Applications*, 21(7), 92. <https://doi.org/10.1038/s41377-018-0094-x>
- Wilt, B. A., Burns, L. D., Wei Ho, E. T., Ghosh, K. K., Mukamel, E. A., & Schnitzer, M. J. (2009). Advances in light microscopy for neuroscience. *Annual Review of Neuroscience*, 32, 435–506. <https://doi.org/10.1146/annurev.neuro.051508.135540>
- Yang, Y., Zhang, Y., Hong, H., Liu, G., Leigh, B. R., & Cai, W. (2011). In vivo near-infrared fluorescence imaging of CD105 expression during tumor angiogenesis. *European Journal of Nuclear Medicine and Molecular Imaging*, 38(11), 2066–2076. <https://doi.org/10.1007/s00259-011-1886-x>
- Yashiro, H., Nakahara, I., Funabiki, K., & Riquimaroux, H. (2017). Microendoscopic system for functional assessment of neural circuits in deep brain regions: Simultaneous optical and electrical recordings of auditory responses in mouse's inferior colliculus. *Neuroscience Research*, 119, 61–69. <https://doi.org/10.1016/j.neures.2017.01.002>
- Zhang, Y., Xie, M., Xue, R., Tang, Q., Zhu, X., Wang, J., Yang, H., & Ma, C. (2021). A novel cell morphology analyzer application in head and neck cancer. *International Journal of General Medicine*, 3(14), 9307–9314. <https://doi.org/10.2147/IJGM.S341420>
- Zhong, W., Celli, J. P., Rizvi, I., Mai, Z., Spring, B. Q., Yun, S. H., & Hasan, T. (2009). In vivo high-resolution fluorescence microendoscopy for ovarian cancer detection and treatment monitoring. *British Journal of Cancer*, 101(12), 2015–2022. <https://doi.org/10.1038/sj.bjc.6605436>

SUPPORTING INFORMATION

Additional supporting information can be found online in the Supporting Information section at the end of this article.

How to cite this article: Nuerbahati, A., Liao, J., Lyu, J., Abduwali, S., & Chiang, L.-Y. (2024). An actively stabilized, miniaturized epi-fluorescence widefield microscope for real-time observation in vivo. *Microscopy Research and Technique*, 1–8. <https://doi.org/10.1002/jemt.24493>